Featured in Physics

Phonon Laser in the Quantum Regime

T. Behrle,[1,*] T. L. Nguyen,[1,‡] F. Reiter,[1,2] D. Baur,[1] B. de Neeve,[1] M. Stadler,[1] M. Marinelli,[1,§] F. Lancellotti,[1] S. F. Yelin,[2] and J. P. Home[1,3,†]

[1]*Institute for Quantum Electronics, ETH Zürich, Otto-Stern-Weg 1, 8093 Zürich, Switzerland*
[2]*Harvard University, 17 Oxford Street, Cambridge, Massachusetts 02138, USA*
[3]*Quantum Center, ETH Zürich, 8093 Zürich, Switzerland*

(Received 24 January 2023; accepted 30 May 2023; published 28 July 2023)

We demonstrate a trapped-ion system with two competing dissipation channels, implemented independently on two ion species cotrapped in a Paul trap. By controlling coherent spin-oscillator couplings and optical pumping rates we explore the phase diagram of this system, which exhibits a regime analogous to that of a (phonon) laser but operates close to the quantum ground state with an average phonon number of $\bar{n} < 10$. We demonstrate phase locking of the oscillator to an additional resonant drive, and also observe the phase diffusion of the resulting state under dissipation by reconstructing the quantum state from a measurement of the characteristic function.

DOI: 10.1103/PhysRevLett.131.043605

Dissipation is intrinsic to quantum systems. While generally being viewed as an obstacle to implementing quantum control, it has also been shown to offer a resource for quantum state preparation and even quantum error correction [1–21]. In the context of many-body physics, dissipation has been shown to lead to phase transitions many of which do not occur in fully coherent systems [5,22–34]. This makes it interesting to explore quantum simulation devices in which dissipation can be tuned precisely to explore all aspects of the physics [35–42]. Realizing such dissipative simulators requires precise control of the coupling between the quantum degrees of freedom and the dissipation channels. When multiple dissipation channels are used, the broadband nature of relaxation processes also produces stringent demands on crosstalk [43].

One archetypal example of a system in which dissipation plays a key role is the laser, which exhibits a dissipative phase transition from a dark phase into a bright phase characterized by the emergence of a coherent state with a random initial phase which diffuses over time. The parameters governing this transition are the photon loss rate (from the cavity mirrors) and gain due to the interaction with the gain medium, which saturates. While in general lasers operate with a gain medium featuring a large number of pumped systems [44,45], lasers have also been built at the single qubit level, e.g., using a single natural [46] or artificial atom [47]. Similar physics to the laser has been observed in mechanical oscillators. Such "phonon lasers" have been realized in a range of systems spanning from atoms to nanomechanics [48–54] with the lasing phase exhibiting a limit cycle of large classical oscillations. In atomic systems these amplitudes were tens of microns in size, corresponding to a mean value of 10^4 phonons.

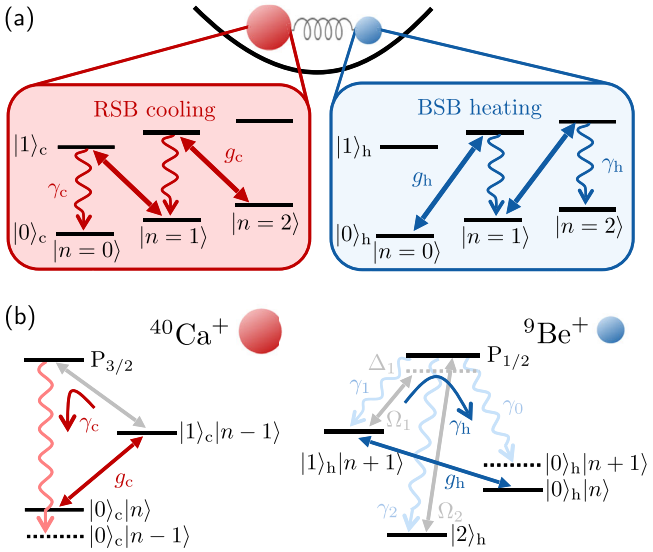

FIG. 1. (a) Schematic of the two dissipative channels. The red (blue) sideband plus engineered decay is applied to calcium (beryllium) and thus realizes cooling (heating) of the shared motional mode. (b) Sketch of heating and cooling process including the engineered decay in calcium and beryllium.

In this Letter, we implement competing dissipation channels with low crosstalk using a two-species ion chain. We use this to investigate the realization of a phonon laser which differs from earlier implementations by operating in the resolved-sideband regime at phonon occupations of $\bar{n} < 10$. This system exhibits three distinct phases, one of which corresponds to phonon lasing. We characterize these by extracting the number state distributions [55]. In the lasing phase, we demonstrate phase locking and phase

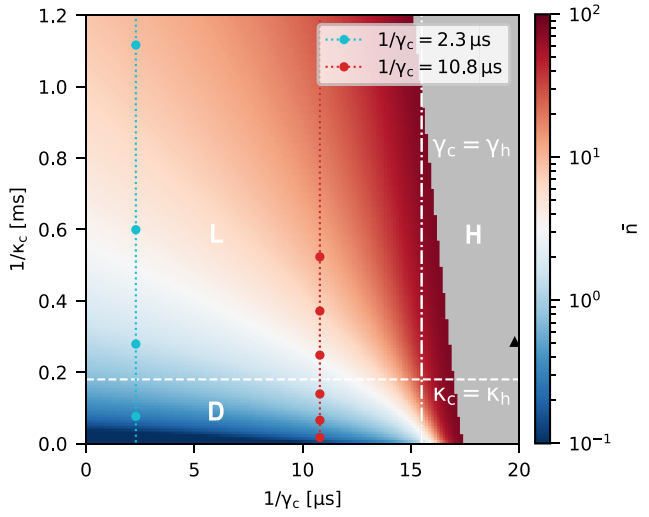

FIG. 2. Simulated phase diagram plotted as a function of control parameters, with the average phonon number used to characterize the steady state. The values are generated using numerical simulations including up to 100 motional states, solving for the steady state. γ_c is the internal state damping rate in the cooling ion while $1/\kappa_c = \gamma_c/g_c^2$, with the sideband coupling strength g_c. An effective beryllium decay $1/\gamma_h = 15.5$ μs and $1/\kappa_h = 0.18$ ms are fixed. Red and light blue dots correspond to the data taken and shown in Fig. 3. White lines indicate the expected phase transitions at $\gamma_c = \gamma_h$ and $\kappa_c = \kappa_h$. Values of $\bar{n} > 80$ are grayed out, they correspond to heating or high $\bar{n}$ lasing values.

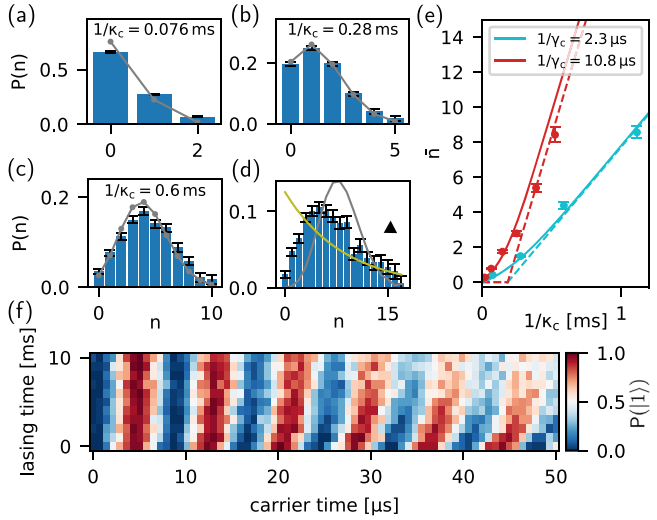

FIG. 3. Phonon distributions for different $1/\kappa_c$. (a)–(c) taken at $1/\gamma_c = 2.3$ μs, show an increase in the average phonon number with an increase of $1/\kappa_c$. The measured phonon distributions (blue bars) agree well with a Poisson distribution of same $\bar{n}$ (gray). (d) Taken in the heating region at $1/\kappa_c = 0.28$ ms and $1/\gamma_c = 19.9$ μs as indicated by the black triangle. Here, the reconstructed phonon distribution neither follows a thermal (green) nor a coherent (gray) distribution of the same $\bar{n}$. (e) Average phonon number as a function of $1/\kappa_c$, mean-field theory (dashed line), simulation (solid line), and experiment (dots with error bars) obtained from the phonon distributions. (f) Calcium carrier oscillations (driving $|0\rangle_c|n\rangle \leftrightarrow |1\rangle_c|n\rangle$) taken in the heating region corresponding to (d). The decrease in calcium carrier frequency for increasing lasing times shows the heating nature.

diffusion, diagnosing these effects by measuring the characteristic function of the motional phonon mode [56].

Our setup [43] takes advantage of the spectral separation for the resonant transitions of beryllium relative to calcium ions, which allows excellent individual addressing for both coherent and dissipative optical pumping control fields. Coupling of the internal states to the shared motional modes is provided by a Jaynes-Cummings (JC) Hamiltonian $\hat{H}_c = \hbar g_c(\hat{a}^\dagger\hat{\sigma}_-^c + \hat{a}\hat{\sigma}_+^c)$ applied to the optical qubit in the calcium ion, and an Anti-Jaynes-Cummings (AJC) Hamiltonian applied to a hyperfine qubit in beryllium $\hat{H}_h = \hbar g_h(\hat{a}^\dagger\hat{\sigma}_+^h + \hat{a}\hat{\sigma}_-^h)$, where $\hat{a}$ is the annihilation operator of the motional mode and $\hat{\sigma}_-^{h/c}$ the lowering operator of the internal state of the heating/cooling ion. The dissipation channels described by the Lindblad jump operators $\hat{L}_{h/c} = \sqrt{\gamma_{h/c}}\hat{\sigma}_-^{h/c}$ are implemented using optical pumping via ancillary short-lived states. The combination of coherent and dissipative driving leads to competing motional cooling (index c) from the calcium ion and motional heating (index h) from beryllium as illustrated in Fig. 1(a). We note that while the gain in our system comes from the use of an AJC Hamiltonian for beryllium allied to internal state pumping from a higher to a lower energy level, a relabeling of internal state levels produces a JC Hamiltonian plus internal state population inversion, as is commonly found in lasers.

To understand the system, we compare it with a mean-field model which makes the assumption of a separation of timescales between fast dynamics in the internal states and slower evolution of the oscillator. The resulting equation for $A = \langle\hat{a}\rangle$ (for which the derivation is given in the Supplemental Material [57]) is

$$\frac{d}{dt}A(t) = A(t)\left(\frac{2\kappa_h}{1 + s_h|A(t)|^2} - \frac{2\kappa_c}{1 + s_c|A(t)|^2}\right), \quad (1)$$

with the gain/loss coefficients $\kappa_{h/c} = g_{h/c}^2/\gamma_{h/c}$, and saturation coefficients $s_{h/c} = 8\kappa_{h/c}/\gamma_{h/c}$ which govern the saturation of the atomic inversion $\propto 1/(1 + s_{h/c}|A(t)|^2)$. This equation allows us to identify separate behaviors which are consistent with a more complete numerical modeling which produces the steady state phase diagram shown in Fig. 2. For $G = \kappa_h/\kappa_c < 1$, the cooling rate of calcium overcomes any heating, and the ground state is a steady state. For $s_h/s_c > G$ (which is equivalent to $\gamma_h/\gamma_c < 1$) it is the only steady state ("dark" region (D) in Fig. 2), while for $s_h/s_c < G$ (equivalent to $\gamma_h/\gamma_c > 1$) an additional set of parameters produces $\dot{A} = 0$, but this regime is unstable to fluctuations. Where the gain exceeds

loss ($G > 1$) the system is above threshold, and the ground state is unstable. Here two distinct regimes exist. The first, occurring for $s_h/s_c > G$ is analogous to lasing (L), in which saturation of the heating process leads to a stable steady state for finite excitation $|A|^2$. The second regime occurs when the cooling ion saturates at lower excitations than the heating ion $s_h/s_c < G$, which leads to a runaway heating effect (H). This latter behavior is not observed in a standard continuous-wave laser system, where the loss is due to leakage from the laser cavity and does not saturate, but has been postulated for driven-dissipative systems dominated by spin decay [33].

We examine these regimes experimentally by applying appropriate Hamiltonians and dissipation until the system attains the steady state, and subsequently characterizing the resulting states through reconstruction of the phonon number distribution. Coherent control is implemented in calcium using a narrow-linewidth laser near resonance with the red sideband of the motional common mode $\omega_m = 2\pi \times 1.8$ MHz of the quadrupole transition $|0\rangle_c \equiv |S_{1/2}, M_J = +1/2\rangle_c \leftrightarrow |1\rangle_c \equiv |D_{5/2}, M_J = +3/2\rangle_c$ at 729 nm. The coupling coefficient in the Lamb-Dicke approximation is given by $g_c = \eta_c \Omega_c$ with the Rabi frequency Ω_c proportional to the electric field gradient of the laser light and the Lamb-Dicke parameter $\eta_c = 0.05$. For beryllium the coupling is produced by a Raman transition near resonance with the blue motional sideband of the qubit transition $|0\rangle_h \equiv |S_{1/2}, F = 2, M_F = +2\rangle_h \leftrightarrow |1\rangle_h \equiv |S_{1/2}, F = 1, M_F = +1\rangle_h$. Here, $g_h = \eta_h \Omega_h$ where Ω_h is proportional to the product of the electric fields of the two Raman lasers and a Lamb-Dicke parameter $\eta_h = 0.15$.

The dissipation channel $\hat{L}_{h/c} = \sqrt{\gamma_{h/c}}\hat{\sigma}_-^{h/c}$ in both ions is provided by laser-driven optical pumping of dipole transitions; see Fig. 1(b). For calcium, this is performed using a resonant laser field with a wavelength of 854 nm which primarily couples $|1\rangle_c$ to $|P_{3/2}, M_J = 3/2\rangle$, from where decay to $|0\rangle_c$ occurs by spontaneous emission. A low fraction of leakage to other levels is mitigated by additional repumping laser fields at 397 nm and 866 nm, not shown. For beryllium, optical pumping from $|1\rangle_h$ to $|0\rangle_h$ uses circularly polarized light which couples $|1\rangle_h$ to the short-lived $P_{1/2}$ excited state. The branching ratio for decay from the excited P state into $|0\rangle_h$ is only one third, with additional decay back into $|1\rangle_h$ and $|2\rangle_h = |S_{1/2}, F = 2, M_F = +1\rangle_h$. We use an additional strong 313 nm beam resonant with $|2\rangle_h \rightarrow |P_{1/2}, F = 2, M_F = 2\rangle_h$ to repump this population and detune the $|1\rangle_h \rightarrow P_{1/2}$ laser by 10 MHz to avoid the formation of a coherent dark state. The four-level nature of the repumping in beryllium results in an additional dephasing of the $|0\rangle_h$ and $|1\rangle_h$ states which is not captured by $\hat{L}$ in the two-level description. We find that the effect of the four levels is captured by an additional dissipation operator $\hat{L}_1 = \sqrt{\gamma_e}|1\rangle_h\langle 1|_h$ at rate $\gamma_e = f\gamma_h$ (with $f = 50/40$ representing the ratio of decay strengths from the P state to $|1\rangle_h$ rather than to $|0\rangle_h$). In the equations above this has the effect of modifying κ_h to $\kappa_h = g_h^2/(\gamma_e + \gamma_h)$. All numerical simulations displayed use the full four-level beryllium dynamics.

In experiments, we fix the parameters for the beryllium (heating) ion, choosing to vary κ_c, s_c through control of calcium. State reconstruction is performed using standard methods, utilizing the number-state dependence of Rabi oscillations on the motional sidebands of the calcium ion [16,55]. We take two slices of the phase diagram using settings which take two distinct values of $1/\gamma_c$. For each value, we extract phonon distributions for several values of $1/\kappa_c$ (y axis of phase diagram). Observed phonon distributions are presented in Figs. 3(a)–3(d), with the obtained mean phonon number shown in Fig. 3(e). We note that the latter increases as κ_h/κ_c transitions from being below to above one, indicating a change from a dark to lasing steady state. Agreement is observed with respect to numerical simulations (solid line) using the calibrated parameters and with respect to predictions of mean-field calculations (dashed line)—these parameters and the calibration methods are given in the Supplemental Material [57]. The obtained phonon distribution in (a) exhibits a peak in $P(n)$ at the origin, whereas in (b) and (c) the distributions are close to those of a Poisson distribution (shown in gray) with the same mean phonon number, which is expected from a coherent state generated by lasing. We also observe the increased saturation of the heating ion (beryllium) as the system transitions to lasing, for instance in the $1/\gamma_c = 2.3$ μs dataset the measured steady state spin population increases from $\langle\hat{\sigma}_z^h\rangle = -0.60$ to $\langle\hat{\sigma}_z^h\rangle = -0.26$ as κ_c is decreased.

As γ_c is decreased relative to γ_h, we reach the heating phase in which the phonon distribution does not attain a steady state. Data from a phonon distribution taken in this regime and sampled at a finite time are shown in Fig. 3(d) and show that the resulting state neither follows a thermal (green) nor a coherent (gray) distribution of the same mean phonon number. Since the system does not reach a steady state, we do not only reconstruct the phonon distribution after a finite time but accompany this by probing Rabi oscillations on the $|0\rangle_c|n\rangle \leftrightarrow |1\rangle_c|n\rangle$ carrier transition (for which the Rabi rate is dependent on the phonon occupation [61]) as a function of the dissipation time—data of this type are shown in Fig. 3(f). Here we observe continued slowing of the Rabi oscillation and reduction of coherence as a function of time, indicating that the mean and variance of the phonon distribution increase.

We also reconstruct states in phase space through the characteristic function $\mathcal{C}(\beta)$ following Ref. [56]. The results are shown in Figs. 4(a) and 4(b). Figure 4(e) shows the marginals of the Wigner function $\mathcal{W}(\alpha)$ for a state with $\bar{n} \approx 4.2$, obtained from the characteristic function by a discrete Fourier transform. These are accompanied by the results of a steady state numerical solution of the Lindblad

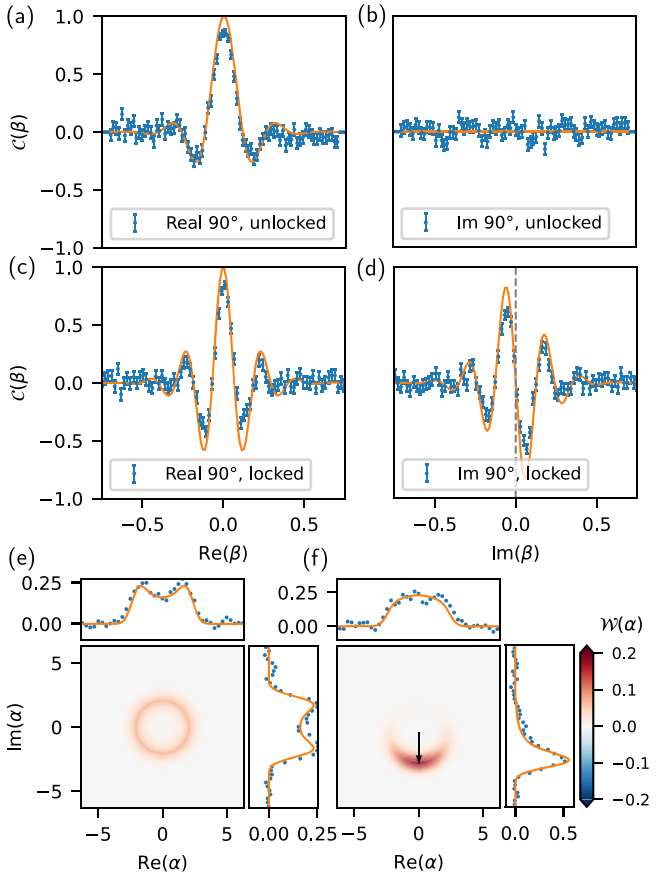

FIG. 4. (a)–(d) Simulation (orange line) and experimental data (blue dots) of real and imaginary part of the characteristic function along the 90 degree axis in the unlocked (a),(b) and locked (c),(d) case. Symmetry breaking in the imaginary part (b) to (d) is observed. (e),(f) Simulated Wigner function (2D) and marginal probability (side plots, orange line) along two axes for the (e) unlocked and (f) phase locked phonon laser including experimental data (blue dots).

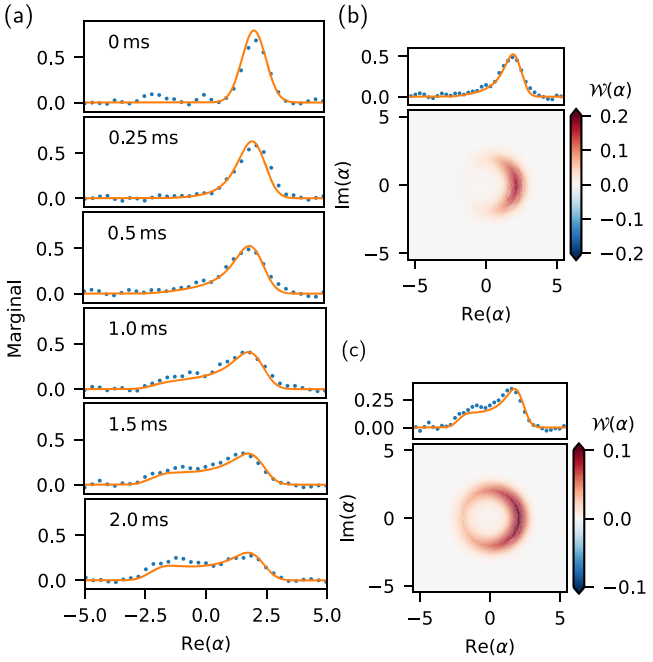

FIG. 5. Phase diffusion. (a) Marginal probabilities along 90 degree axis for different lasing lengths. Starting from a coherent state with a well-defined phase, the lasing process introduces phase diffusion over time (simulation in orange, experiment in blue). (b),(c) Simulated Wigner functions (2D) with marginal probabilities for a dissipation duration of 0.5 ms and 1.5 ms.

master equation. The phase symmetry can be broken by adding an external drive of a well-defined phase to which the oscillator locks. We introduce such a drive by applying a resonant oscillating force to the oscillator using a voltage applied to a trap electrode, resulting in a Hamiltonian $\hat{H}_t = \hbar g(\hat{a}e^{i\Phi_t} + \hat{a}^\dagger e^{-i\Phi_t})$. The force strength $g = 2\pi \times 0.4$ kHz is chosen to be weak enough such that it does not overwhelm the lasing dynamics. Figures 4(c) and 4(d) show data for the characteristic function measured with the force on. Figure 4(f) shows the corresponding marginals of the Wigner function. The experimental data agree well with numerical simulations performed using experimentally observed parameters, which are plotted alongside. Clear symmetry breaking in the imaginary part of the characteristic function is observed from Figs. 4(b)–4(d). From comparison with the simulated Wigner function, we see that the state is nevertheless not perfectly represented by a coherent state, with some phase diffusion being visible.

To investigate phase diffusion during the dissipation, we examine the effects on an initial coherent state which has the same $\bar{n} \approx 4.2$ as the steady state but a well-defined phase. Figure 5(a) shows the marginals of the Wigner distribution along the real axis, which show the effects of diffusion. The results from numerical simulations (orange line) using a four-level beryllium system and two levels for calcium with parameters obtained using independent calibration experiments agree with the data (blue dots), and allow us to extract a linear increase in the phase uncertainty with time at a rate of $\langle \dot{\theta}^2 \rangle = 0.022$ rads^2/s. This diffusion is analogous to that which produces the Schawlow-Townes limit for the laser linewidth [45,62]. We find that this agrees with numerical simulations, but Heisenberg-Langevin calculations seem to overestimate the diffusion, for reasons which we do not understand [57].

The work performed here differs in two important aspects from earlier work on phonon lasing with trapped ions [48]. First, the phonon occupation is lower, stemming from the use of the resolved-sideband regime. Hence, our results sit at the boundary where quantum effects are accessible, and methods are available for extracting this information, such as characteristic function and Fock-state reconstruction. Second, there are fundamental differences in the physics. In earlier work, which used a transition in a single ion driven simultaneously at two frequencies, the

balance between heating and cooling appeared due to nonlinearity in the ion-light interaction caused by the modification of the line shape for large Doppler shifts, with no saturation of the internal state. Here, by contrast, the saturation of the "gain" ion is what introduces nonlinearity.

The experiments above use a relatively simple pair of dissipation channels, involving single-frequency laser tones applied in the Hamiltonian part of the control. By using multifrequency drives, similar experiments could explore reservoirs for which the underlying state space is more easily described in a squeezed or displaced Fock basis. This extension would provide a realization of a squeezed phonon laser, which has been predicted to offer advantages in sensing [63–65]. Extensions of competing reservoir systems to multiple ions would allow for the realization of more generalized spin-boson models such as the open Dicke model.

T. B. and T. L. N. performed the experiments, with experimental support from B. N., M. S., M. M., and F. L. Theoretical preparatory work was performed by T. L. N. and F. R. with support from J. H. Data analysis was performed by T. B. and T. L. N. Theoretical understanding of the results was produced by D. B., T. B., F. R., S. F. Y., and J. H. The paper was written by T. B. and J. H. with input from all authors. We acknowledge support from the Swiss National Science Foundation (SNF) under Grant No. 200020 179147/1, the SNF through the National Centre of Competence in Research for Quantum Science and Technology (QSIT) Grant No. 51NF40–185902, the SNF Ambizione Grant No. PZ00P2-186040, and the EU Quantum Flagship H2020-FETFLAG-2018-03 Grant No. 820495 AQTION. S. F. Y. would like to acknowledge funding from the NSF through the CUA PFC.

*tbehrle@phys.ethz.ch
†jhome@phys.ethz.ch
‡Present address: QuantX Labs Pty Ltd, Adelaide, Australia.
§Present address: JILA, Boulder, Colorado, USA.

[1] J. I. Cirac, A. S. Parkins, R. Blatt, and P. Zoller, Phys. Rev. Lett. **70**, 556 (1993).
[2] J. F. Poyatos, J. I. Cirac, and P. Zoller, Phys. Rev. Lett. **77**, 4728 (1996).
[3] A. R. R. Carvalho, P. Milman, R. L. de Matos Filho, and L. Davidovich, Phys. Rev. Lett. **86**, 4988 (2001).
[4] F. Verstraete, M. M. Wolf, and J. I. Cirac, Nat. Phys. **5**, 633 (2009).
[5] S. Diehl, A. Micheli, A. Kantian, B. Kraus, H. P. Büchler, and P. Zoller, Nat. Phys. **4**, 878 (2008).
[6] B. Kraus, H. P. Büchler, S. Diehl, A. Kantian, A. Micheli, and P. Zoller, Phys. Rev. A **78**, 042307 (2008).
[7] F. Pastawski, L. Clemente, and J. I. Cirac, Phys. Rev. A **83**, 012304 (2011).
[8] H. Krauter, C. A. Muschik, K. Jensen, W. Wasilewski, J. M. Petersen, J. I. Cirac, and E. S. Polzik, Phys. Rev. Lett. **107**, 080503 (2011).
[9] J. T. Barreiro, M. Müller, P. Schindler, D. Nigg, T. Monz, M. Chwalla, M. Hennrich, C. F. Roos, P. Zoller, and R. Blatt, Nature (London) **470**, 486 (2011).
[10] Y. Lin, J. P. Gaebler, F. Reiter, T. R. Tan, R. Bowler, A. S. Sørensen, D. Leibfried, and D. J. Wineland, Nature (London) **504**, 415 (2013).
[11] S. Shankar, M. Hatridge, Z. Leghtas, K. M. Sliwa, A. Narla, U. Vool, S. M. Girvin, L. Frunzio, M. Mirrahimi, and M. H. Devoret, Nature (London) **504**, 419 (2013).
[12] A. Sarlette, J. M. Raimond, M. Brune, and P. Rouchon, Phys. Rev. Lett. **107**, 010402 (2011).
[13] C. Navarrete-Benlloch, J. J. García-Ripoll, and D. Porras, Phys. Rev. Lett. **113**, 193601 (2014).
[14] A. Kronwald, F. Marquardt, and A. A. Clerk, Phys. Rev. A **88**, 063833 (2013).
[15] V. Jarlaud, P. Hrmo, M. K. Joshi, and R. C. Thompson, J. Phys. B **54**, 015501 (2020).
[16] D. Kienzler, H.-Y. Lo, B. Keitch, L. de Clercq, F. Leupold, F. Lindenfelser, M. Marinelli, V. Negnevitsky, and J. P. Home, Science **347**, 53 (2015).
[17] M. Malinowski, C. Zhang, V. Negnevitsky, I. Rojkov, F. Reiter, T.-L. Nguyen, M. Stadler, D. Kienzler, K. K. Mehta, and J. P. Home, Phys. Rev. Lett. **128**, 080503 (2022).
[18] B. de Neeve, T.-L. Nguyen, T. Behrle, and J. P. Home, Nat. Phys. **18**, 296 (2022).
[19] M. E. Kimchi-Schwartz, L. Martin, E. Flurin, C. Aron, M. Kulkarni, H. E. Tureci, and I. Siddiqi, Phys. Rev. Lett. **116**, 240503 (2016).
[20] Y. Lu, S. Chakram, N. Leung, N. Earnest, R. K. Naik, Z. Huang, P. Groszkowski, E. Kapit, J. Koch, and D. I. Schuster, Phys. Rev. Lett. **119**, 150502 (2017).
[21] E. Zapusek, A. Javadi, and F. Reiter, Quantum Sci. Technol. **8**, 015001 (2022).
[22] E. M. Kessler, G. Giedke, A. Imamoglu, S. F. Yelin, M. D. Lukin, and J. I. Cirac, Phys. Rev. A **86**, 012116 (2012).
[23] S. Morrison and A. S. Parkins, Phys. Rev. Lett. **100**, 040403 (2008).
[24] N. Lang and H. P. Büchler, Phys. Rev. A **92**, 012128 (2015).
[25] T. E. Lee, F. Reiter, and N. Moiseyev, Phys. Rev. Lett. **113**, 250401 (2014).
[26] S. Genway, W. Li, C. Ates, B. P. Lanyon, and I. Lesanovsky, Phys. Rev. Lett. **112**, 023603 (2014).
[27] H. J. Carmichael, Phys. Rev. X **5**, 031028 (2015).
[28] J. Hannukainen and J. Larson, Phys. Rev. A **98**, 042113 (2018).
[29] M.-J. Hwang, P. Rabl, and M. B. Plenio, Phys. Rev. A **97**, 013825 (2018).
[30] F. Brennecke, R. Mottl, K. Baumann, R. Landig, T. Donner, and T. Esslinger, Proc. Natl. Acad. Sci. U.S.A. **110**, 11763 (2013).
[31] M. Buchhold, P. Strack, S. Sachdev, and S. Diehl, Phys. Rev. A **87**, 063622 (2013).
[32] P. Werner, K. Völker, M. Troyer, and S. Chakravarty, Phys. Rev. Lett. **94**, 047201 (2005).
[33] F. Reiter, T. L. Nguyen, J. P. Home, and S. F. Yelin, Phys. Rev. Lett. **125**, 233602 (2020).

[34] F. E. Öztürk, T. Lappe, G. Hellmann, J. Schmitt, J. Klaers, F. Vewinger, J. Kroha, and M. Weitz, Science **372**, 88 (2021).
[35] T. Fink, A. Schade, S. Höfling, C. Schneider, and A. Imamoglu, Nat. Phys. **14**, 365 (2018).
[36] J. M. Fink, A. Dombi, A. Vukics, A. Wallraff, and P. Domokos, Phys. Rev. X **7**, 011012 (2017).
[37] F. Couëdo, O. Crauste, A. A. Drillien, V. Humbert, L. Bergé, C. A. Marrache-Kikuchi, and L. Dumoulin, Sci. Rep. **6**, 35834 (2016).
[38] R. Ma, B. Saxberg, C. Owens, N. Leung, Y. Lu, J. Simon, and D. I. Schuster, Nature (London) **566**, 51 (2019).
[39] M. Fitzpatrick, N. M. Sundaresan, A. C. Y. Li, J. Koch, and A. A. Houck, Phys. Rev. X **7**, 011016 (2017).
[40] S. R. K. Rodriguez, W. Casteels, F. Storme, N. Carlon Zambon, I. Sagnes, L. Le Gratiet, E. Galopin, A. Lemaître, A. Amo, C. Ciuti, and J. Bloch, Phys. Rev. Lett. **118**, 247402 (2017).
[41] F. Bibak, U. Delić, M. Aspelmeyer, and B. Dakić, Phys. Rev. A **107**, 053505 (2022).
[42] F. Reiter, F. Lange, S. Jain, M. Grau, J. P. Home, and Z. Lenarčič, Phys. Rev. Res. **3**, 033142 (2021).
[43] V. Negnevitsky, M. Marinelli, K. K. Mehta, H.-Y. Lo, C. Flühmann, and J. P. Home, Nature (London) **563**, 527 (2018).
[44] R. Loudon, *The Quantum Theory of Light* (Oxford University Press, Oxford, 2000).
[45] M. O. Scully and M. S. Zubairy, *Quantum Optics* (Cambridge University Press, Cambridge, England, 1997).
[46] J. McKeever, A. Boca, A. D. Boozer, J. R. Buck, and H. J. Kimble, Nature (London) **425**, 268 (2003).
[47] O. Astafiev, K. Inomata, A. O. Niskanen, T. Yamamoto, Y. A. Pashkin, Y. Nakamura, and J. S. Tsai, Nature (London) **449**, 588 (2007).
[48] K. Vahala, M. Herrmann, S. Knünz, V. Batteiger, G. Saathoff, T. W. Hänsch, and T. Udem, Nat. Phys. **5**, 682 (2009).
[49] I. S. Grudinin, H. Lee, O. Painter, and K. J. Vahala, Phys. Rev. Lett. **104**, 083901 (2010).
[50] U. Kemiktarak, M. Durand, M. Metcalfe, and J. Lawall, Phys. Rev. Lett. **113**, 030802 (2014).
[51] J. D. Cohen, S. M. Meenehan, G. S. MacCabe, S. Gröblacher, A. H. Safavi-Naeini, F. Marsili, M. D. Shaw, and O. Painter, Nature (London) **520**, 522 (2015).
[52] R. M. Pettit, W. Ge, P. Kumar, D. R. Luntz-Martin, J. T. Schultz, L. P. Neukirch, M. Bhattacharya, and A. N. Vamivakas, Nat. Photonics **13**, 402 (2019).
[53] Y. Wen, N. Ares, F. J. Schupp, T. Pei, G. A. D. Briggs, and E. A. Laird, Nat. Phys. **16**, 75 (2020).
[54] Q. Zhang, C. Yang, J. Sheng, and H. Wu, Proc. Natl. Acad. Sci. U.S.A. **119**, e2207543119 (2022).
[55] D. M. Meekhof, C. Monroe, B. E. King, W. M. Itano, and D. J. Wineland, Phys. Rev. Lett. **76**, 1796 (1996).
[56] C. Flühmann and J. P. Home, Phys. Rev. Lett. **125**, 043602 (2020).
[57] See Supplemental Material at http://link.aps.org/supplemental/10.1103/PhysRevLett.131.043605 for further information, which includes Refs. [18,45,56,58–60].
[58] F. Reiter and A. S. Sørensen, Phys. Rev. A **85**, 032111 (2012).
[59] J. J. Bollinger, J. S. Wells, D. J. Wineland, and W. M. Itano, Phys. Rev. A **31**, 2711 (1985).
[60] A. E. Siegman, *Lasers* (University Science Books, Sausalito, California, 1986).
[61] D. Wineland, C. Monroe, W. Itano, D. Leibfried, B. King, and D. Meekhof, J. Res. Natl. Inst. Stand. Technol. **103**, 259 (1997).
[62] A. L. Schawlow and C. H. Townes, Phys. Rev. **112**, 1940 (1958).
[63] S. Fernández-Lorenzo and D. Porras, Phys. Rev. A **96**, 013817 (2017).
[64] P. A. Ivanov, Phys. Scr. **95**, 025103 (2020).
[65] Y.-Q. Wei, Y.-Z. Wang, Z.-C. Liu, T.-H. Cui, L. Chen, J. Li, S.-Q. Dai, F. Zhou, and M. Feng, Sci. China Phys. Mech. Astron. **65**, 110313 (2022).